

# Different Cooling Rates and Their Effect on Morphology and Transformation Kinetics of Martensite

Annika Eggbauer (Vieweg), Gerald Ressel, Marina Gruber, Petri Prevedel, Stefan Marsoner, Andreas Stark, and Reinhold Ebner

## Abstract

The characteristics of martensitic transformation is strongly dependent on the cooling rate applied to the material. For a quenched and tempered steel, the martensitic transformation occurs below 500 °C, but in industry, cooling rates are normally characterized for cooling in the temperature regime between 800 and 500 °C. The effects of different cooling rates in the lower temperature regime were thus, not intensively investigated in the past. To this end, a 50CrMo4 steel is quenched in a dilatometer applying varying cooling rates below 500 °C. The martensite microstructure is analyzed by APT, TEM and EBSD in regard to carbon distribution, lath width and block sizes. Additionally, hardness measurements are carried out and martensite start temperatures as well as the retained austenite phase fractions are evaluated. It can be shown, that lowering the cooling rate leads to increased carbon segregation within the martensitic matrix. The main effect is a decrease in martensite hardness. Also the block size increases with lower cooling rate.

## Keywords

Cooling parameter • Cooling rate • Martensite Auto tempering • Quenched and tempered steel

## Introduction

Steel offers the possibility to achieve a diversity of microstructures and mechanical properties just by adapting the cooling program from the austenitic state. For a conventional quenched and tempered (QT) steel, fast cooling procedures lead to a hard martensitic microstructure, while slow air cooling causes a soft ferritic-pearlitic microstructure [1–3].

For industrial applications the cooling rate is often specified by means of the cooling parameter  $\lambda$ , which is defined as the time passing from 800 to 500 °C divided by 100 [1]. Looking into typical time temperature transformation diagrams (Fig. 1) it becomes obvious that the time from 800 to 500 °C is important for the transformation of austenite to phases such as ferrite or pearlite. For a martensitic microstructure, however, the cooling parameter is solely defining the cooling rate needed to avoid bainite or ferrite phase formation. However, below 500 °C there is still room for a diversity of cooling strategies to achieve a fully martensitic microstructure. Since for common quenched and tempered steels the martensite start temperature ( $M_s$ ) is around 300 °C, cooling below 500 °C will continue to affect the formation of martensite.

Martensitic transformations are defined as diffusionless transformations, although local atomic diffusion might occur to some extent within the martensitic state at high temperatures during the cooling procedure. This behavior is described as auto-tempering [4]. Carbon can either segregate to lattice defects or, if cooling is sufficiently slow, carbides, e.g. cementite, are formed. Both segregation and precipitation can lead to different martensitic properties, such as hardness and toughness in the as-quenched state.

A. Eggbauer (Vieweg) (✉) · G. Ressel · M. Gruber  
P. Prevedel · S. Marsoner · R. Ebner  
Materials Center, Leoben Forschung GmbH, Leoben, Austria  
e-mail: Annika.Vieweg@mcl.at; Annika.eggbauer@mcl.at

G. Ressel  
e-mail: Gerald.Ressel@mcl.at

M. Gruber  
e-mail: Marina.Gruber@mcl.at

P. Prevedel  
e-mail: Petri.Prevedel@mcl.at

S. Marsoner  
e-mail: Stefan.Marsoner@mcl.at

R. Ebner  
e-mail: Reinhold.Ebner@mcl.at

A. Stark  
Helmholtz Zentrum Geesthacht, Geesthacht, Germany  
e-mail: andreas.stark@hzg.de

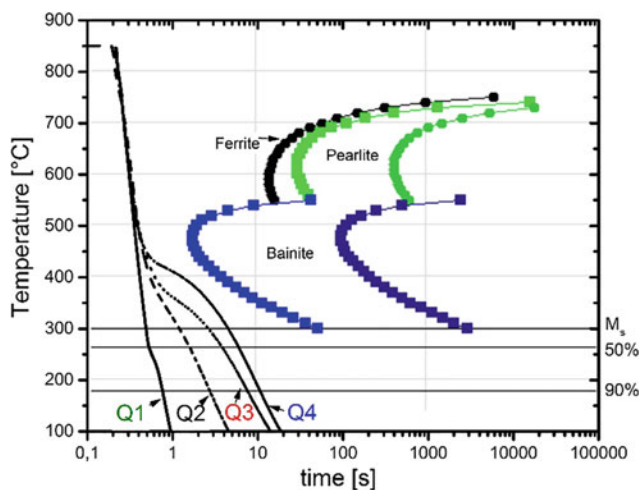


**Fig. 1** Time temperature transformation (TTT-) diagram for the investigated steel grade calculated with JMAT Pro<sup>TM</sup>. Black circles correspond to 0.1% ferrite, light green circles to 0.1% pearlite and dark green circles to 99.9% pearlite. Light blue squares refer to 0.1% bainite and dark blue squares to 99.9% bainite. The experimental cooling curves Q1 (solid line), Q2 (dashed line), Q3 (dotted line) and Q4 (dashed-dotted line) are depicted within the diagram

Furthermore, the tempering kinetics might change for different martensitic structures.

Therefore, this study discusses the differences within the martensitic microstructure as a consequence of different cooling strategies below 500 °C in regard to segregation and auto-tempering phenomena as well as transformation kinetics. To analyze the differences, a comprehensive set of high resolution methods such as dilatometry, 3D atom probe tomography (3D-APT), transmission electron microscopy (TEM), electron back scattered diffraction (EBSD) as well as high energy X-ray diffraction (HEXRD) is used.

## Experimental

The investigated steel in this study was a 50CrMo4-steel with 0.49 wt% C, 0.71 wt% Mn, 1.05 wt% Cr, 0.18 wt% Mo, 0.27 wt% Si, 0.02 wt% P and 0.01 wt% S.

For dilatometer experiments, cylindrical samples with a diameter of 4 mm and a length of 10 mm were manufactured at half radius of a rolled material.

The heat treatments were conducted using a DIL 805L/A dilatometer from TA Instruments (formerly BAEHR).

Austenitization of all samples was done at 850 °C for 20 min. To obtain different quenching rates, the gas flow during quenching was either set to maximum (Q1) or was regulated according to the specific programs (Q2-Q4). The quenching rate from 850 to 500 °C was constant (2300 K/s,  $t = 0.15$  s) for all experiments. All cooling programs were conducted twice and exhibited equal phase transformation behavior. The different cooling procedures are depicted in Fig. 1, which shows a time temperature transformation (TTT) diagram calculated with JMAT Pro<sup>TM</sup> for the analyzed steel grade. Table 1 lists the cooling times from 500 to 300 °C ( $t_{500/300}$ ), from  $M_s$  to 100 °C ( $t_{M_s/100}$ ) and the overall cooling time from 850 to 100 °C ( $t_{850/100}$ ). The dilatometer data were analyzed to determine the volume fraction of martensite using the lever rule. To apply the lever rule, linear fits for austenite were done between 500 and 300 °C, linear fits for martensite between 100 and 50 °C for all data.

The TEM analysis was carried out on a FEI Tecnai F20, equipped with a field emission gun at an accelerating voltage of 200 kV. The samples were electrochemically etched on a Struers Tenupol 5, using a 7% solution of perchloric acid at temperatures around -10 °C. In order to achieve reasonable statistics, lath widths were determined by acquiring and evaluating 10 TEM images of each condition, hence around 150 laths were evaluated per condition.

The 3D-APT measurements were carried out at a LEAP<sup>TM</sup> System 3000XHR in voltage mode at a temperature of 60 K with a pulse frequency of 200 kHz and a pulse fraction of 20%. The tips were reconstructed using the IVAS 3.6.8. software tool provided by CAMECA.

Block sizes were analysed using electron backscattered diffraction (EBSD). Samples were ion-polished using a Hitachi IM4000plus ion milling device. EBSD measurements were carried out with a Zeiss Auriga cross beam workstation by investigating an area of  $70 \times 70 \mu\text{m}$  and a step size of 50 nm. The data were analysed using the Orientation Imaging Microscopy (OIM) data analysis software from EDAX and subsequently the data was cleaned using grain dilatation, with a dilation angle of  $10.5^\circ$  (as seen to be the best fit for martensitic materials in literature [5])

To obtain the amount of retained austenite, diffraction patterns of the samples were acquired by means of high energy X-ray diffraction (HEXRD) measurements at the HEMS beamline (P07) at Petra III [6]. For these measurements, the as-quenched martensitic microstructures were

**Table 1** Nomenclature of the different cooling strategies.  $t_{500/300}$  time gives the cooling time from 500 to 300 °C,  $t_{M_s/100}$  from  $M_s$  to 100 °C and  $t_{850/100}$  from 850 to 100 °C

Name	$t_{500/300}$ [s]	$t_{M_s/100}$ [s]	$t_{850/100}$ [s]
Q1	0.13	0.4	0.59
Q2	0.8	3	3.95
Q3	2.2	10.5	12.85
Q4	4.1	12.9	17.15

placed into the beam at room temperature with an exposure time of 0.2 s. In order to penetrate the 4 mm thick samples, high energy X-rays were used with a photon energy of 87.1 keV, corresponding to a wavelength of 0.14235 Å. The beam size was 0.7 × 0.7 mm. The resulting diffraction rings were recorded with a Perkin Elmer XRD1621 flat panel detector. The data were integrated using the fit2D software from ESRF [7]. Retained austenite amounts were analyzed using TOPAS 4-2 and the Rietveld Method [8]. The hardness measurements were performed on a Qness Q10A+ Vickers hardness tester.

## Results

The dilatometer data were evaluated in regard to the transformation kinetics using the lever rule. The evolution of the martensite volume fraction over temperature is depicted in Fig. 2 for the four different cooling strategies. Differences in

“zero” level occur due to the evaluation method, since all data were fitted in the same temperature region, this is not a transformation effect. Only distinct bends are real transformation phenomena. Figure 2 shows that no significant difference in martensite start temperature ( $M_s$ ) occurs for the different cooling strategies. Little variations are subject to deviation of the analysis method, hence  $M_s$  is at  $267 \pm 2$  °C. Nevertheless, Q3 and Q4 show a slight increase in volume fraction of martensite prior to  $M_s$  (around 290 °C). This increase is more pronounced for Q4 than for Q3. Additionally, Q1 seems to exhibit the lowest slope at the beginning of the transformation.

Lath widths as well as block sizes are analyzed and depicted in Fig. 3a. The lath width (closed squares) remains constant around 0.2 μm for all samples. The measuring uncertainty of this evaluation method is large, so no trend can be stated. However, with increasing cooling time the block size (open circles) is significantly increasing from 2 to 2.5 μm. Due to the little differences in blocksize values, Q1

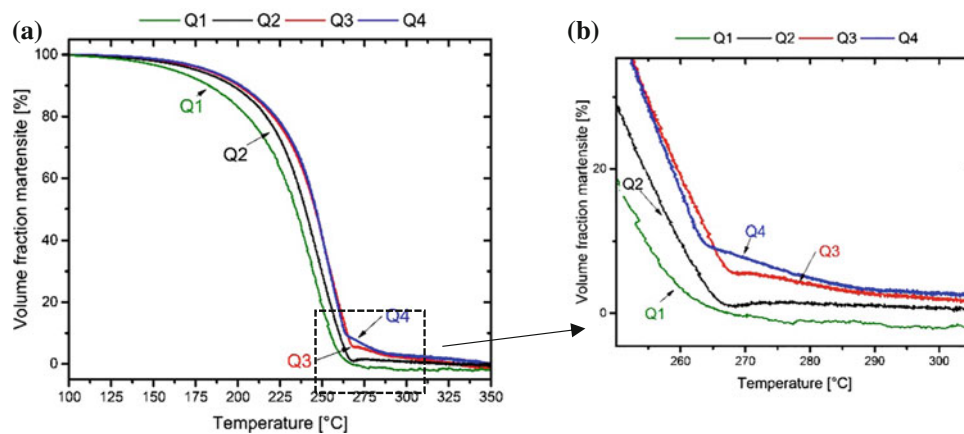


**Fig. 2** Amount of martensite in vol% as a function of the temperature determined by means of the lever rule applied on the dilatometer data (a) and the region of interest around  $M_s$  in detail (b)

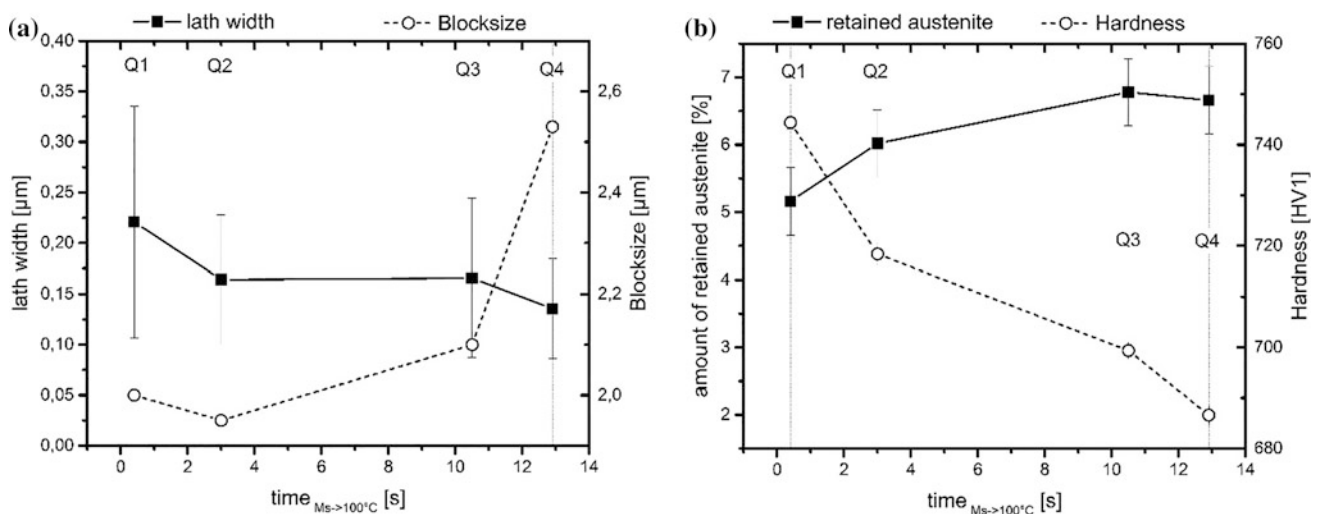


**Fig. 3** Lath width (closed squares) and block size (open circles) depicted against the time from  $M_s$  to 100 °C (a); Amount of retained austenite (closed squares) and hardness (open circles) over time from  $M_s$  to 100 °C (b)

and Q2 are stated to be within the same range of 2  $\mu\text{m}$ , and the decrease in block-size is due to deviations across the analyzed area.

Another important aspect for the as-quenched state is the amount of retained austenite, shown in Fig. 3b by means of closed squares. The amount of retained austenite is slightly increasing from 5.2 to 6.7% with increasing cooling time. In

contrast to this trend, the hardness is significantly decreasing and drops from 744 HV1 for Q1 to 686 HV1 for Q4. An evaluation of the HEXRD patterns (not depicted) does not reveal indications for the occurrence of cementite in any of the as-quenched states. Additionally, the lattice constants of the austenite and ferrite were evaluated but no trend between the four states can be stated.

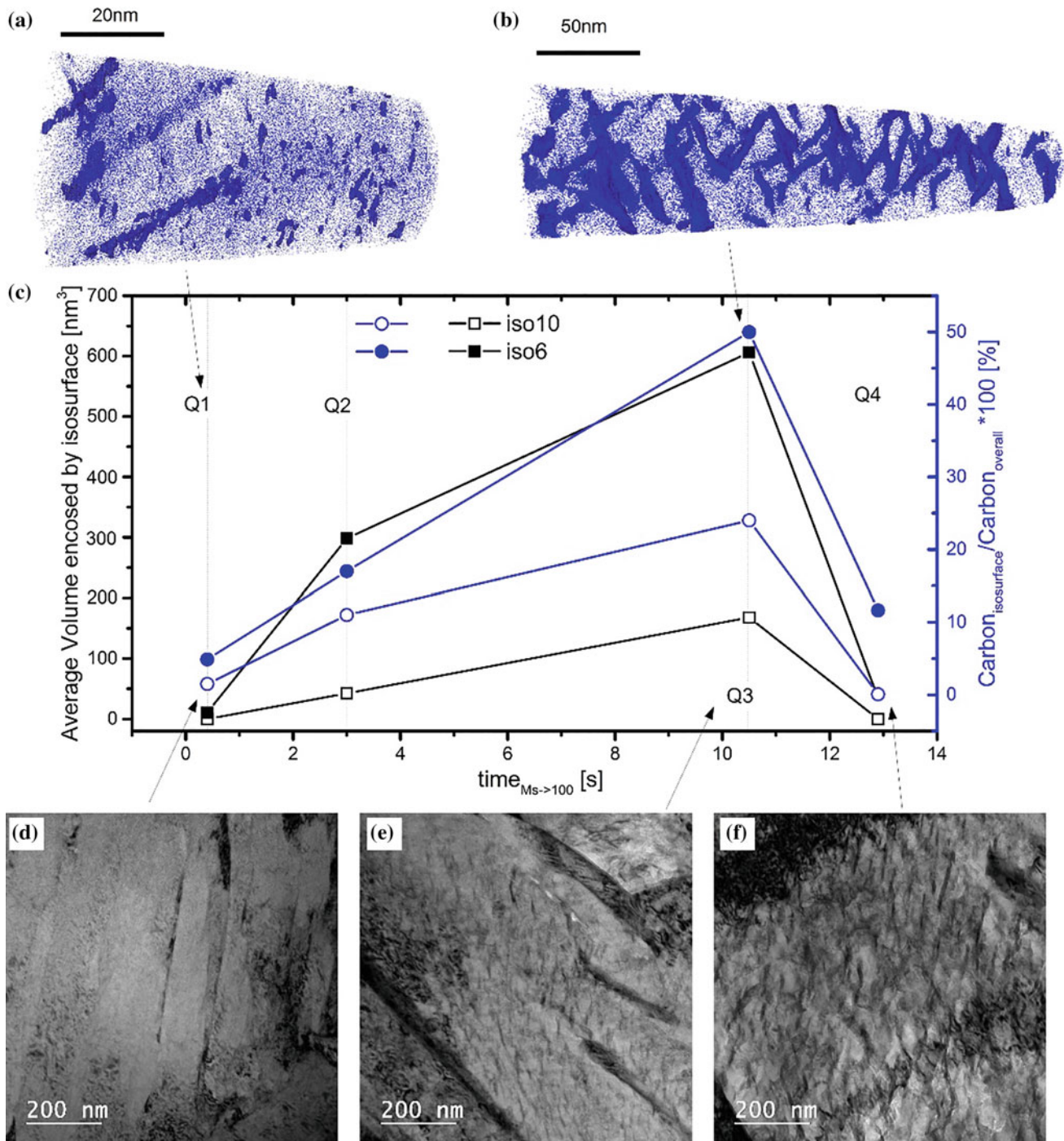


**Fig. 4** Carbon enrichment indicated by means of isosurfaces of 6 (closed symbols) and 10 at.% carbon (open symbols) and by the ratio carbon within isosurface/overall carbon evaluated from the APT

samples and selected 3D atom probe tips (c). Additionally, APT tips of Q1 (a) and Q3 (b) are depicted. Additionally, TEM bright field images of Q1 (d), Q3 (e) and Q4 (f) are depicted

To analyze the carbon segregation as a function of the cooling rate 3D-APT measurements were conducted. To this end, isosurfaces of 6 (closed symbols) and 10 at.% carbon (open symbols) were analyzed in regard to their volume (black squares) and the amount of carbon within these isosurfaces in relation to the overall amount of carbon ions (blue circles) within the tip. The results can be seen in Fig. 4c. For better imagination, the APT tips of Q1 (Fig. 4a) and Q3 (Fig. 4b) are depicted as well. The overall amount of carbon within the investigated martensite laths was 2.1 (Q1, Q3), 2.3 (Q2) and 2.6 at.% C (Q4). The differences are due to rolling segregation across the material, but are still in the range of the nominal composition of the steel (2.23 at.% C). The features of the isosurfaces are developed along bands, in a cylindrical manner. It is clearly visible, that the amount of carbon within the isosurfaces in relation to the overall carbon ions, as well as the average volume of the isosurfaces, is increasing from Q1 to Q3. For Q4 these attributes drastically drop to a value between Q1 and Q2, due to less isosurfaces within this condition. Furthermore, also by visual inspection an enrichment of carbon within the isosurfaces as well as a coarsening can be observed for Q1–Q3. In order to analyze carbon segregation, transmission electron microscopy was conducted and bright field (BF) images of Q1 (d) Q3 (e) and Q4 (f) are depicted in Fig. 4. While for Q1 nothing is visible inside the lath, Q3 and Q4 show increased precipitations within the laths. These precipitations did not show any scattering within selected area diffraction, hence no indexing could be done.

## Discussion

The cooling strategies were chosen to avoid any other phase transformation than the martensitic one. The bainite phase nose visible in Fig. 1 was not passed by the cooling curves. Nevertheless, phase fraction analysis in Fig. 2 show the presence of a second transformation for the two slowest cooling strategies Q3 and Q4. It can be assumed, that the calculated TTT diagram differs from the real transformation behavior determined by dilatometry for the actual chemical composition of the investigated steel since a slight bainitic phase transformation is visible. Nevertheless,  $M_s$  was not quantifiably affected by the different cooling strategies below 500 °C.

The martensitic transformation itself is diffusionless [9], however, significant diffusion of carbon can occur in the formed martensite during subsequent quenching. Since all carbon enrichments within the APT tips, occur along lines and little round features are detected within the conditions, segregation of carbon is present [10]. Once a martensite lath is formed carbon can segregate to lattice defects which act as traps for carbon. The segregated areas can subsequently act as

nucleation sites for carbides, i.e. cementite [10]. As the segregation and formation of carbides is dependent on diffusion, their size and overall content depend on the martensite start temperature as well as on the cooling rate. As a result, at constant  $M_s$  temperature higher cooling rates lead to shorter diffusion paths of carbon and consequently to a lower amount of segregations. This is confirmed by the APT measurements, since the highest cooling rate shows a low amount of carbon within the segregations and also a smaller fraction of segregations compared to the conditions Q2 and Q3.

The sample of the condition Q4 shows less segregation as well as lower carbon isosurface value within the APT tips compared to the conditions Q3 and Q2. This trend was reproduced over several tips. Comparing the TEM images of Q1, Q3 and Q4 (Fig. 4) it is obvious, that segregation is increasing with increasing cooling time. Q4 shows segregations [10]. The amount of carbon trapped at dislocations is depending on the overall amount of carbon as well as the dislocation density [11]. Due to less dislocations within Q4, less segregated areas are present. Using APT the distances between the segregations are increasing so that APT shows less segregation due to the small size of the tips. However, due to the small volume measured in APT, segregations might obtain a longer distance than APT is able to detect. Therefore, it is possible, that none of the increased segregated areas was evaluated. Concluding, attention needs to be paid evaluating segregated areas using APT, due to the very local evaluation.

Despite the fact, that the prior austenite grain size is equal in all samples, since austenitization was always done equally, the block size is decreasing with decreasing cooling time (Fig. 3a). Blocks form within a packet which is built through a shift along the same habit plane [5, 12]. At higher temperatures austenite yield strength is lower [13] and hence it is assumed, that its resistance against lattice displacement (i.e. martensite formation) is decreased. As evaluated through Fig. 2, phase transformation obtains a higher slope around  $M_s$  for slower cooling rates, meaning a higher transformation rate. The martensite formed at higher temperatures is forming within an austenite with lower yield strength compared to lower temperatures. Consequently, larger martensite packets can be formed, since the resistance against crystallographic shift is lower at elevated temperatures (close to  $M_s$ ) compared to lower temperatures. This leads to larger packets for slow cooling rates. At higher cooling rates, higher undercooling takes place (visible through the lower slope after  $M_s$  for Q1) and the dwell time at higher temperatures is thus limited. The crystallographic shift occurs at multiple habit planes simultaneously and due to the increasing yield strength of the austenite with decreasing temperature the shifted area is decreased. This leads to increased amounts of packets per austenite grain and, therefore, smaller packets. Smaller packets

subsequently lead to a smaller block size [12, 14]. Consequently, high cooling rates lead to smaller block sizes.

From the experimental results of this work it can be derived that faster cooling of martensite results in higher hardness. This higher hardness is caused by a combination of three effects. The most dominant reason for the higher hardness can be related to minimized segregation of carbon to lattice defects upon fast cooling, as can be observed within the APT tips in Fig. 4. Consequently the distortion of ferrite crystal reaches a maximum. For Q4 the dislocation density is assumed to be lower than for Q1 and Q2, hence the matrix is less distorted through dislocation relieve during cooling and consequently softer. Secondly, the decreasing block size with decreasing cooling time can strengthen the matrix according to Hall-Petch [15, 16]. A correlation of mechanical properties of martensitic materials and the block size of lath martensite is an essential factor in the strength-structure relationship [17, 18]. Finally, the lower amount of retained austenite (Fig. 3b) causes a less decrease of the hardness of the material. However, this effect is assumed to be the least dominant (only around 10 HV10), concluding from the rule of mixture (hardness of austenite  $\sim 100$  HV10, hardness of martensite  $\sim 800$  HV10).

## Conclusions

This work shows that during the quenching process of a 50CrMo4 steel the cooling rate below 500 °C has essential influence on the resulting martensitic microstructure. Therefore, it should be chosen carefully to obtain the desired martensite properties, such as hardness, in the as-quenched material. Special focus needs also to be drawn to possible bainitic phase transformations prior martensite formation. To sum up, the following conclusions can be drawn:

- The hardness is increasing with decreasing cooling time. This is due to three main effects being the increased crystal lattice distortion due to less segregated carbon and higher dislocation density, increasing block size and decreasing amounts of retained austenite
- The martensite start temperature is not influenced by the cooling rate below 500 °C. A slight transformation before  $M_s$  is detected for the two slowest cooling procedures. This is supposed to be due to (beginning) bainite formation.
- Due to dislocation recovery during slow cooling, less dislocations are present for segregation, hence the distance between the segregated areas increases and APT measurements are no longer accurate.
- The block size is increasing with increasing cooling time below 500 °C, since less undercooling occurs and larger packets can shift from one habit plane due to lower austenite resistance at higher temperatures.

**Acknowledgements** Financial support by the Austrian Federal Government (in particular from Bundesministerium für Verkehr, Innovation und Technologie and Bundesministerium für Wissenschaft, Forschung und Wirtschaft) represented by Österreichische Forschungsförderungsgesellschaft mbH and the Styrian and the Tyrolean Provincial Government, represented by Steirische Wirtschaftsförderungsgesellschaft mbH and Standortagentur Tirol, within the framework of the COMET Funding Programme is gratefully acknowledged. The TEM investigations were carried out using facilities at the University Service Centre for Transmission Electron Microscopy, Vienna University of Technology, Austria. The authors want to thank Jozef Keckes for the help with the synchrotron measurements and Francisca Martin Mendez for the help with the 3D APT measurements.

## References

1. Totten GE, Howes MA (1997) Steel heat treatment handbook. CRC Press
2. Bleck W (2004) Werkstoffkunde Stahl für Studium und Praxis, 2nd edn. Mainz, Aachen
3. Franz Wever (1961) Atlas zur Wärmebehandlung der Stähle, Teil 1&2. Max-Planck-Institut für Eisenforschung
4. Speich G, Leslie W (1972) Metall Trans 3(5):1043–1054
5. Morito S, Huang X, Furuhashi T, Maki T, Hansen N (2006) Acta Mater 54(19):5323–5331
6. King A, Beckmann F, Müller M, Schreyer A, Schell N, Fischer T (2014) Mechanical stress evaluation by neutrons and synchrotron radiation VI. In: Volume 772 of Materials science forum. Trans Tech Publications, 2, pp 57–61
7. Hammersley AP (1997) Fit2d: an introduction and overview. ESRF internal report, ESRF97HA02T
8. Young RA (1993) The Rietveld method. Oxford University Press, New York
9. Bhadeshia H (2002) Martensite in steel
10. Vieweg A, Povoden-Karadeniz E, Ressel G, Prevedel P, Wojcik T, Martin-Mendez F, Stark A, Keckes J, Kozeschnik E (2017) Mater Des 136:214–222
11. Fischer FD, Svoboda J, Kozeschnik E (2013) Modell Simul Mater Sci Eng 21(2):025008
12. Morito S, Tanaka H, Konishi R, Furuhashi T, Maki T (2003) Acta Mater 51(6):1789–1799
13. Byun TS, Hashimoto N, Farrell K (2004) Acta Mater 52(13):3889–3899
14. Hanamura T, Torizuka S, Tamura S, Enokida S, Takechi H (2013) ISIJ Int 53(12):2218–2225
15. Hall E (1951) Proc Phys Soc Sect B 64(9):747
16. Petch NJ (1953) Iron Steel Inst 174:25–28
17. Morito S, Yoshida H, Maki T, Huang X (2006) Mater Sci Eng: A 438–440(0):237–240. In: Proceedings of the international conference on martensitic transformations
18. Morris E (2001) The influence of grain size on the mechanical properties of steel